Colloid Polym Sci (2004) 282: 802–809
DOI 10.1007/s00396-004-1125-0

ORIGINAL CONTRIBUTION

In situ synchrotron SAXS/WAXD studies during melt spinning of modified carbon nanofiber and isotactic polypropylene nanocomposite

Shaofeng Ran
Christian Burger
Igors Sics
Kyunghwan Yoon
Dufei Fang
Kwangsok Kim
Carlos Avila-Orta
Jongkahk Keum
Benjamin Chu
Benjamin S. Hsiao
David Cookson
Dave Shultz
Myungae Lee
Jim Viccaro
Yasuo Ohta

Received: 29 January 2004
Accepted: 1 April 2004
Published online: 5 May 2004

Dedicated to Prof. E D. Fischer on his 75th birthday.

S. Ran · C. Burger · I. Sics · K. Yoon
D. Fang · K. Kim · C. Avila-Orta
J. Keum · B. Chu (✉) · B. S. Hsiao
Department of Chemistry,
State University of New York at Stony Brook, Stony Brook, NY 11794-3400, USA
E-mail: bchu@notes.cc.sunysb.edu

D. Cookson · D. Shultz
M. Lee · J. Viccaro
ChemMat CARS, APS, ANL,
9700 South Cass Ave,
Argonne, IL 60439-4859, USA

Y. Ohta
Toyobo Research Center Co. Ltd,
2-1-1 Katata, 520-0292 Otsu, Shiga, Japan

Abstract The structural development of a nanocomposite, containing 95 wt% isotactic polypropylene (iPP) and 5 wt% modified carbon nanofiber (MCNF), during fiber spinning was investigated by in situ synchrotron small-angle X-ray scattering (SAXS) and wide-angle X-ray diffraction (WAXD) techniques. The modification of carbon nanofibers (CNFs) was accomplished by a chemical surface treatment using in situ polymerization of olefin segments to enhance its compatibility with iPP, where the iPP/MCNF nanocomposite was prepared by twostep blending to ensure the dispersion of MCNF. X-ray results showed that at low spin-draw ratios, the iPP/MCNF nanocomposite fiber exhibited much higher iPP crystalline orientation than the control iPP fiber. At higher spin-draw ratios, the crystalline orientation of the nanocomposite fiber and that of the pure iPP fiber was about the same. The crystallinity of the composite fiber was higher than that of the control iPP fiber, indicating the nucleating effect of the modified carbon nanofibers. The nanocomposite fiber also showed larger long periods at low spin-draw ratios. Measurements of mechanical properties indicated that the nanocomposite fiber with 5 wt% MCNF had much higher tensile strength, modulus and longer elongation to break. The mechanical enhancement can be attributed to the dispersion of MCNF in the matrix, which was confirmed by SEM results.

Keyword Carbon nanofiber · Polypropylene · Nanocomposite · Fiber spinning · SAXS · WAXD

Introduction

Single-walled carbon nanotubes (SWNTs) and multi-walled carbon nanotubes (MWNTs) have been suggested as good nanofillers to create a new class of high performance polymers and fibers due to their high strength, lightweight, small diameters (~1 nm for SWNTs and 2~50 nm for MWNTs) and large aspect ratios [1]. In particular, carbon nanotubes-based nanocomposites may offer new opportunities for applications because of the highly anisotropic electronic properties, improved thermal conductivity (higher than diamond), and superior mechanical properties (that surpass the stiffness and strength of any known polymer materials) of carbon nanotubes [2]. However, with the current production technology, carbon nanotubes are still too expensive for practical use. An alternative carbon nanotube-based nanofillers are the much less expensive vapor grown carbon nanofibers (CNFs), which have an average diameter of 50~200 nm, bridging the gap between the diameter of conventional carbon fibers (7~10 μm) and those of SWNTs and MWNTs. Carbon nanofibers can be produced in a relative large scale by the catalytic decomposition of certain hydrocarbons on small metal particles such as iron, cobalt, nickel, and some of their alloys [3, 4, 5, 6].

Recently, several polymer nanocomposites based on CNFs have been demonstrated in the literature, including the systems of isotactic polypropylene (iPP) [7, 8], polycarbonate (PC) [9], and nylon [10]. In these studies, while improvements of mechanical properties were seen, the major hurdle appeared to be the fine balance between the preparation schemes and the dispersion of CNFs in the polymer. The practical melt mixing method is not always effective to disperse the entangled carbon nanofibers, which often forms a dense and robust network structure at high CNF concentrations.

Chemical functionalization is an especially attractive route to increase the solubility of carbon nanotubes in the polymer matrix, which can also facilitate the processability of nanocomposites with conventional melt processing methods. Recently, different functionalization schemes have been reviewed by Hirsch [11], including defect-group functionalization [12, 13, 14], covalent sidewall functionalization [15, 16], non-covalent exohedral [16], and endohedral functionalization [17]. However, functionalization of CNFs to improve the miscibility between CNFs and polyolefins by melt mixing has never been reported.

In this study, the surface of CNFs was modified by in situ polymerization of olefin segments to increase the interfacial compatibility between CNFs and iPP. Nanocomposites containing dispersed modified carbon nanofibers (MCNF) in iPP were prepared by melt blending, which was verified by scanning electron microscopy (SEM). The structural development of the nanocomposite fiber during spinning was followed by in situ synchrotron small-angle X-ray scattering (SAXS) and wide-angle X-ray diffraction (WAXD) techniques, which have recently been developed in our laboratory [18]. Mechanical properties including the Young's modulus, tensile strength and elongation-to-break of the composite fiber were also evaluated, which showed notable improvements over those of iPP fibers with no MCNFs.

Experimental

Materials

The iPP sample was an experimental resin provided by ExxonMobil Chemical Company. The carbon nanofiber (PR-24-HHT) was obtained from Pyrograf Products, Inc. The sample underwent thermal treatment to remove any non-carbon material. The typical morphology of the as-received CNFs is shown in Fig. 1. The as-received CNFs had an average diameter of 70 nm and a length of 50–100 μm (the aspect ratio was thus about 1000). We found that the as received CNFs were clean and free of any remaining catalyst. No additional purification procedures were taken in this study.

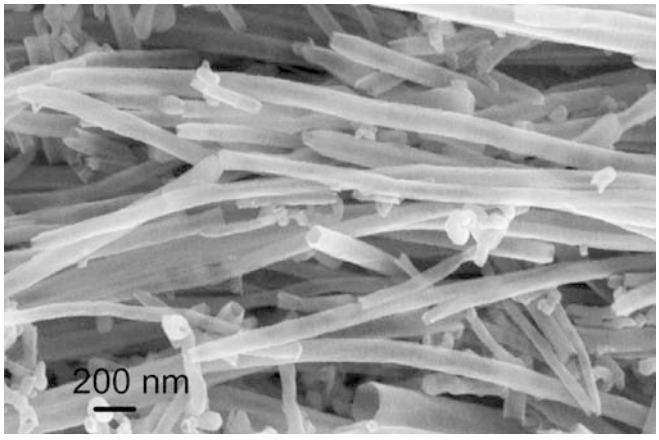

Fig. 1 Morphology of as-received carbon nanofibers (CNFs) by SEM

Surface Modifications of CNFs

All reagents were obtained from Aldrich, and solvents were obtained from Fisher Scientific. Styrene and triethylamine (TEA) were distilled with CaH_2. Tetrahydrofuran (THF) was dried by sodium under nitrogen. Other reagents were used without purification. Silica gel for flash chromatography was Merck grade 60 (70–230). Two polymerization initiators, 1-(benzyloxy)-2-phenyl-2-(2′,2′,6′,6′-tetramethyl-1′-piperidinyloxy)ethane (TEMPO-ester) and 1-hydroxy-2-phenyl-2-(2′,2′,6′,6′-tetramethyl-1′-piperidinyloxy)ethane (TEMPO-alcohol), were synthesized based on the reported procedure [19]. The overall synthetic schemes are summarized as follows, but the details of the synthesis and characterization of MCNFs will be reported later.

(1) Acid group generation on carbon nanofibers The surface acidic groups (carboxylic acid and hydroxyl) on the carbon nanofibers were generated by the oxidation reaction using potassium perchlorate/sulfuric acid solution (e.g., 2 g of carbon nanofibers in $KClO_3$ solution (i.e., 2 g of $KClO_3$ in 100 ml of concentrated H_2SO_4)) at room temperature [20]. The carbon nanofiber suspension was filtered using a 0.2-μm filter and washed with de-ionized water and methanol. The filtered nanofibers were dried in vacuo at 70 °C.

(2) Attachment of radical initiator to the carbon nanofiber surfaces The oxidized CNFs were refluxed in thionyl chloride for 24 h at 65 °C. Subsequently, the thionyl chloride was removed by distillation. The dried acyl chloride modified CNFs were reacted with TEMPO-alcohol in dry THF using TEA as a catalyst at 75 °C for two days. The reaction mixture was then washed with water and THF, and then dried in vacuo at 70 °C.

(3) Surface free-radical polymerization The initiator-attached CNFs were mixed with isoprene (the mole ratio

of initiator to monomer was about 1:480) [21]. The mixture was heated at 130 °C for 10 h. After polymerization, the grafted CNFs were washed with methanol and dried in vacuo at 70 °C.

(4) Reduction of the grafted polymer The grafted CNFs were dispersed in xylene. *p*-toluenesulfonyl hydrazide, where tri-*n*-propyl amine was also added to the solution mixture [22]. The mixture was heated to reflux at 140 °C for 4 h. The resultant solution was filtered, washed with de-ionized water and methanol, and dried in vacuo at 90 °C. The overall modification schemes from (1) to (4) are illustrated below 1.

Nanocomposite preparation

In order to obtain good dispersion of MCNF in iPP, a two-step mixing process was used to prepare the iPP/MCNF nanocomposite. The first step involved solution blending, where 5 wt% of MCNF and 95 wt% of iPP were mixed in xylene at 130 °C and then precipitated in cold methanol. The dried precipitates were then melt-blended with about 3 wt% of antioxidant Irgonox 3114 to form the composite using a DACA twin-screw micro-compounder at 190 °C for 3 min.

In situ SAXS/WAXD measurements during fiber spinning

The in situ fiber spinning study was carried out using a custom-built spinning apparatus constructed in our laboratory. A photograph of this spinning apparatus and the WAXD beam line setup at ChemMat CARS of the Advanced Photon Source (APS), Argonne National Laboratory (ANL), is shown in Fig. 2. In this apparatus, a capillary rheometer-like barrel was located on the top platform, which held the polymer melt (e.g., nanocomposite) with an upper temperature capability of about 350 °C. A motor driven plunger was used to extrude the polymer melt out of the barrel and formed fibers. The top platform could be moved vertically, allowing the X-ray detection spot along the spinning line to be changed. The apparatus was mounted on a pair of precision optical rails, which permitted the alignment of the monofilament fiber with the X-ray beam. A take-up wheel with an adjustable speed control provided the means to change the spin-draw ratio (SDR), defined as the ratio of the fiber take-up speed to the extrusion speed at the spinneret exit.

The in-situ fiber spinning experiment was carried out in the ChemMat CARS at APS. The wavelength used was 0.75 Å for WAXD and 1.50 Å for SAXS. The third-generation synchrotron X-ray beam at the APS was sufficiently strong that a 5-s exposure of the monofilament fiber with a diameter of $\backsim$6–10 μm was able to yield excellent SAXS/WAXD images with high signal-to-noise ratios. The real-time measurements during fiber spinning were performed using a Bruker CCD X-ray detector. The distance between the sample center and the detector plane for WAXD was 59.6 mm, as calibrated by an Al_2O_2 standard, and for SAXS 1903 mm, which was calibrated by a collagen standard. The melt-spinning study of iPP/MCNF was

Schemes. 1–4

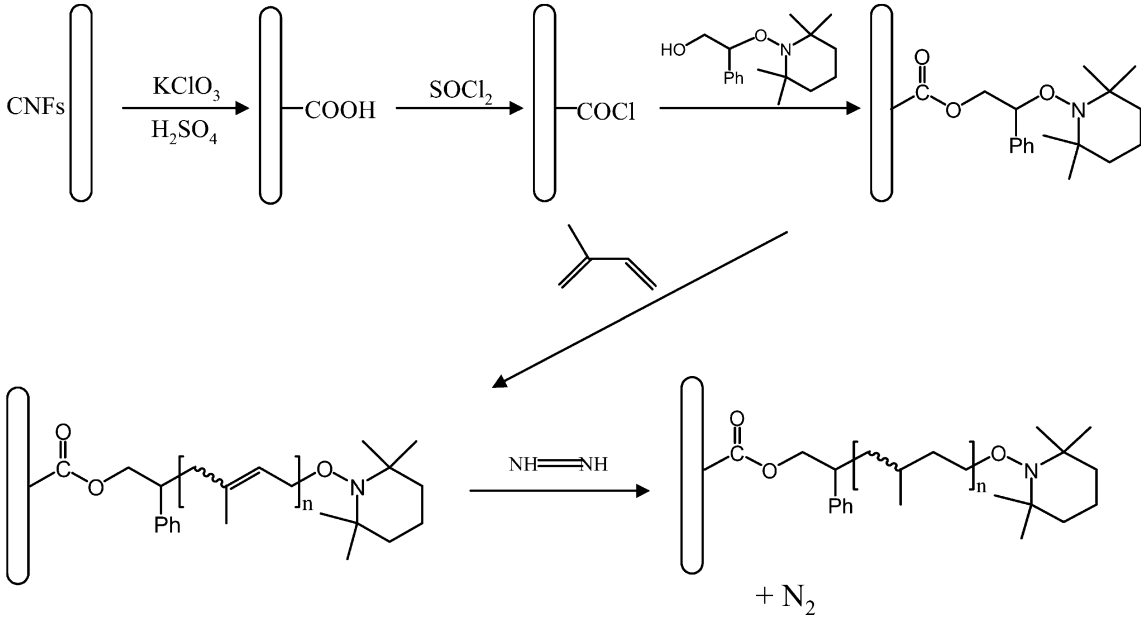

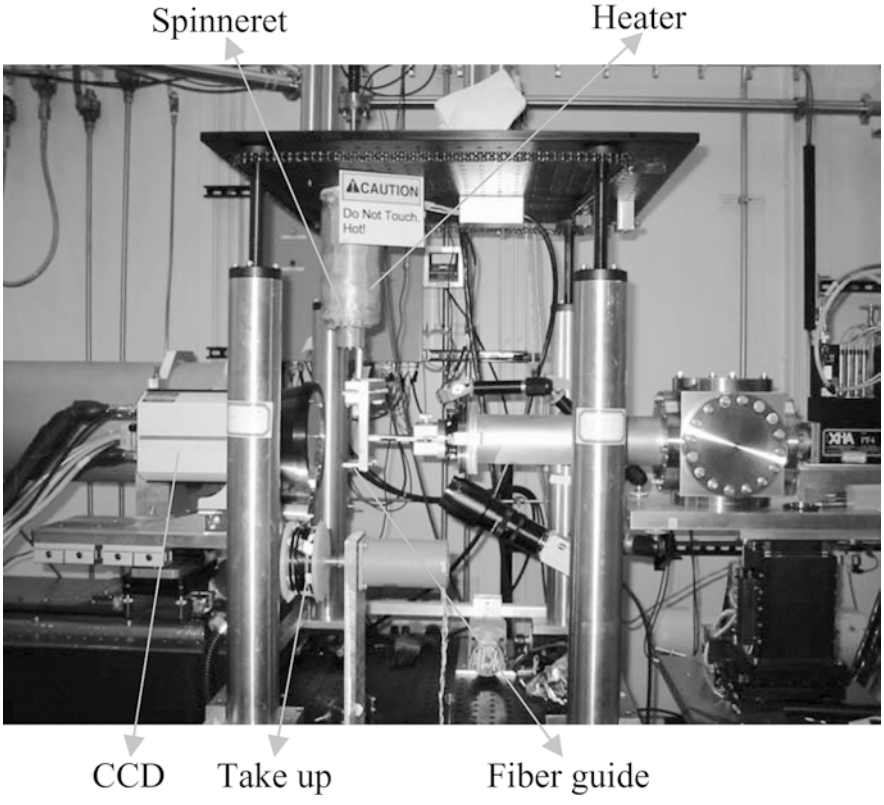

Fig. 2 Synchrotron WAXD setup at ChemMat CARS at APS/ANL for in-situ fiber spinning study

carried out at 195 °C. The extrusion speed of the fiber at the spinneret was fixed at 5.2 mm/s.

SEM measurements

The surface and the cross-section of the iPP/MCNF nanocomposite and pure iPP fibers were studied by scanning electron microscopy (SEM, LEO 1550). The SEM instrument was equipped Schottky field-emission gun (10 kV) and Robinson backscatter detector. The cross-section of the fibers was obtained by fracturing the fibers in liquid nitrogen. All samples received gold coating to minimize charging effect.

Mechanical properties measurements

A bundle of spun fibers, about ten filaments glued by epoxy at two ends, with SDR of 50.0 was used to test the mechanical properties using an Instron stretching apparatus (model 4410). The testing was performed at a constant speed of 20 mm/min at room temperature. The gage length was 10 mm. The tensile strength, Young's modulus, and the elongation-to-break of the iPP/MCNF nanocomposite and pure iPP fibers were determined. Five repeats were done to obtain the average values of the tensile strength, modulus and strain at break.

Results and discussion

Figure 3 shows selected two-dimensional (2D) WAXD patterns of the spun iPP/MCNF composite fiber at different spin-draw ratios after correction of the air scattering. These patterns showed well-resolved diffraction peaks, typical of the α-form iPP crystals. With increasing spindraw ratios, the azimuthal spreads of the reflection peaks became much narrower, indicating that the crystal orientation was improved. Since the diffraction peaks of the pure carbon nanofiber are very close to some of the iPP reflections, it is not easy to distinguish the MCNF from iPP in the composite WAXD patterns at low spin-draw ratios. Fortunately, at high spin-draw ratios (i.e., SDR = 31 and 60), the 002 reflection of CNF was clearly observed because of the difference in the orientation between iPP and MCNF structures. It should be noted that we used the designation "002" only because of its resemblance from the graphite structure. The implied "ABA" stacking sequence of the carbon layers is usually not found in MWNTs or CNFs. It was seen because MCNF was only partially oriented in the nanocomposite at high spin-draw ratios.

One of the advantages in conducting the synchrotron experiments at ChemMat Cars/APS/ANL is that the X-ray wavelength could be easily adjusted. The relatively short wavelength (0.75 Å) chosen in this work

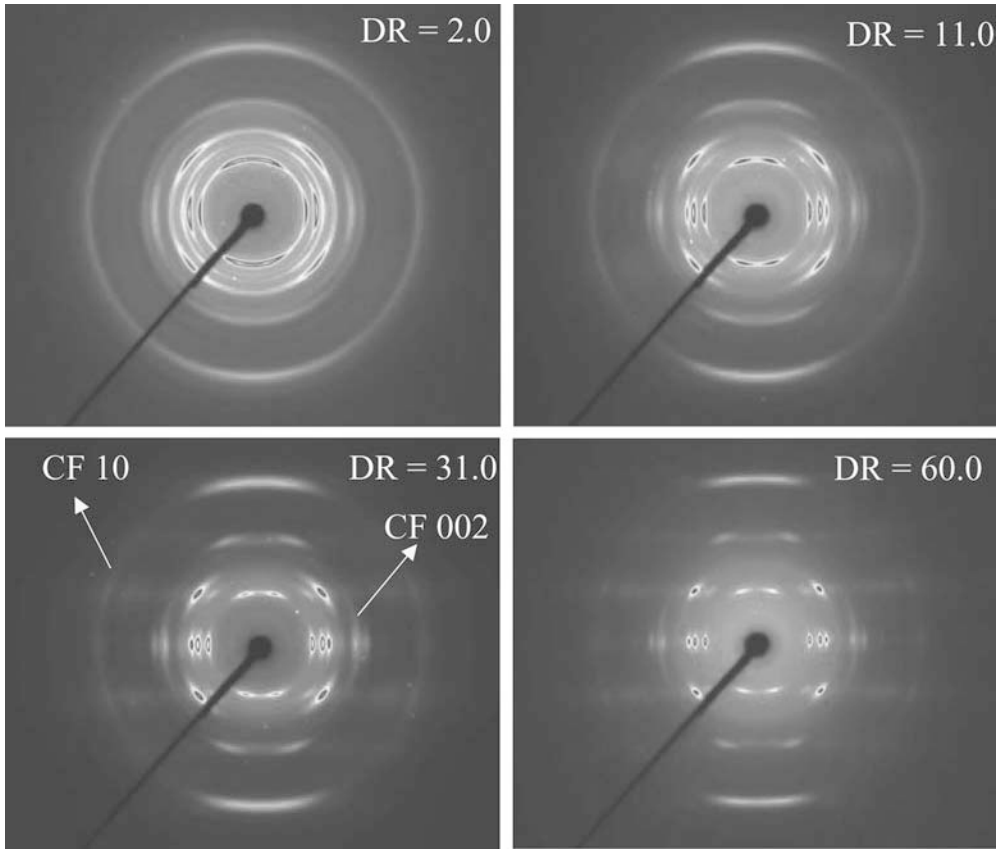

Fig. 3 Two-dimensional WAXD patterns of the nanocomposite fiber at different spin draw ratios after correction of air scattering

allowed both the first (10) and the second (11) intra-graphene-layer reflections of the CNFs to be visible, the latter only as a very weak ring near the limits of the experimental *s*-range. The intra-graphene-layer reflections are indexed as (hk) only due to the absence of inter-layer correlations. It was interesting to note that the orientation of the iPP reflection (040) was much higher than that of the reflection (110) at low spin-draw ratios. At high spin-draw ratios, the orientation of (110) and (040) were almost the same, which indicated that the orientation of (110) and (040) developed differently during fiber spinning. The calculation of the Hermans' orientation factor P_2 of reflections (110) and (040) confirmed this observation. The chain axis orientation in the spun fiber was calculated mathematically by using the following equations [23]:

$$\langle \cos^2 \phi_{c,Z} \rangle = 1 - 1.099 \langle \cos^2 \phi_{110,Z} \rangle - 0.901 \langle \cos^2 \phi_{040,Z} \rangle$$

$$\langle P_2(\cos \phi_{c,Z}) \rangle = \frac{3\langle \cos^2 \phi_{c,Z} \rangle - 1}{2}$$

where Z represents the direction of the fiber axis and c indicates the molecule chain direction.

Figure 4 shows the calculated Hermans' orientation factor P_2 for both nanocomposite fiber and pure iPP fiber. It was found that at low spin-draw ratios, the 5 wt% MCNF reinforced iPP nanocomposite fiber had much higher orientation than the control iPP fiber, indicating that MCNF facilitated the orientation of iPP chains at low spin-draw ratios, which could be due to the reduction of local melt viscosity during spinning. When the spin-draw ratios were high, the orientations of the nanocomposite fiber and the pure iPP fiber were almost

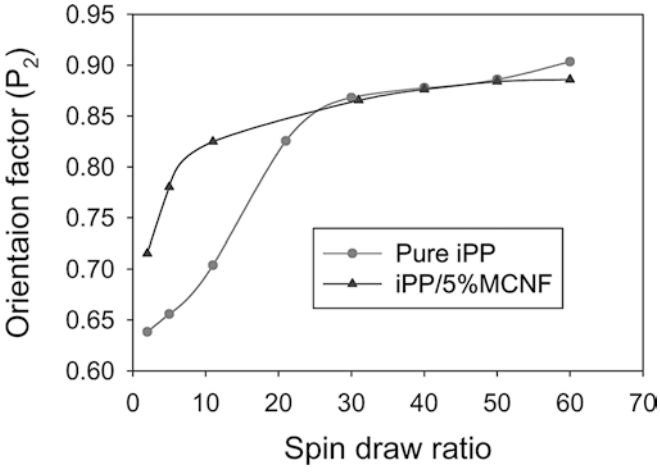

Fig. 4 Hermans orientation factor of chain axis for both nanocomposite and pure iPP fibers at different spin-draw ratios

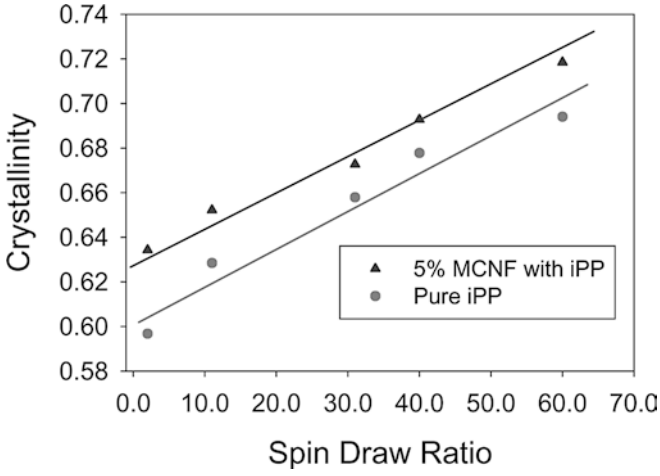

Fig. 5 Crystallinity of the nanocomposite and pure iPP fibers as a function of spin draw ratio

the same, which all reached a very high degree of orientation (i.e., $P_2 = 0.9$ with $P_2 = 1.0$ indicating perfect orientation). Our explanation is that the rigid short carbon nanofibers, which are easily oriented at low spin-draw ratio, can act as anisotropic nucleating sites to enhance the alignment of iPP chains along the drawing direction. In addition, the short olefin chains on the MCNF surface may reduce the local viscosity of the matrix around the vicinity carbon nanofibers. At high spin-draw ratios, all of the iPP chains are highly oriented and the nucleating effects of the carbon nanofibers are no longer significant.

One-dimensional (1D) intensity profiles were extracted from 2D WAXD patterns using a spherical averaging method, taking into account of the proper weighting factor with simple fiber symmetry assumption. These intensity profiles were plotted as a function of the absolute value of the scattering vector $s = 2\sin(\theta)/\lambda$ (λ and 2θ represent wavelength and scattering angle, respectively), from which the crystallinity was estimated using a peak fitting procedure to separate the crystalline peaks and amorphous background. Figure 5 shows the estimated crystallinity of the spun nanocomposite fibers and pure iPP fibers as a function of the spin-draw ratio. It was found that the crystallinity of both nanocomposite and control iPP fibers all increased almost linearly with the spin-draw ratio, which is probably due to the strain-induced crystallization. It was seen that the crystallinity of the nanocomposite fiber was slightly larger than that of the control iPP fiber, which suggests that the modified carbon nanofibers acted as heterogeneous nucleating sites for iPP crystallization.

Figure 6 shows the 2D SAXS patterns of the composite fibers at different spin-draw ratios. The patterns showed a meridionally aligned two-point pattern, indicating the presence of a lamellar structure of iPP with the lamellar normal preferentially aligned with the fiber axis. A second-order of the scattering peak was clearly visible in the higher s range, which requires a certain amount of long-range order of the lamellar structures in the fiber. The long periods ($d = 1/s$) were obtained form the Lorentz-corrected peak maxima.

Figure 7 illustrates the obtained long periods of the nanocomposite and pure iPP fibers as a function of the

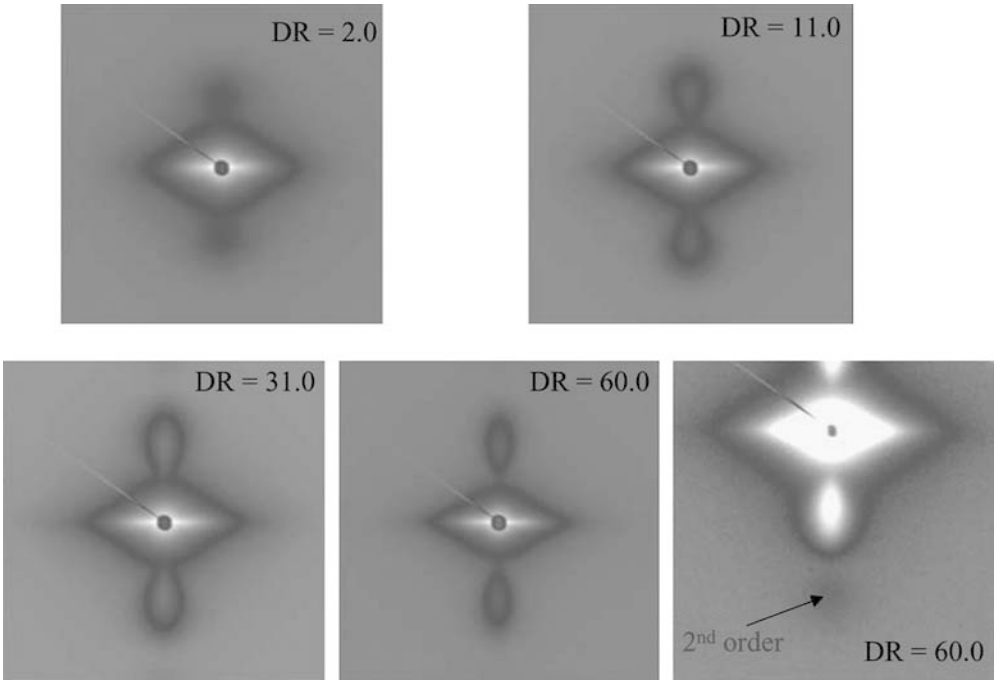

Fig. 6 Two-dimensional SAXS patterns of the nanocomposite fiber at different spin-draw ratios

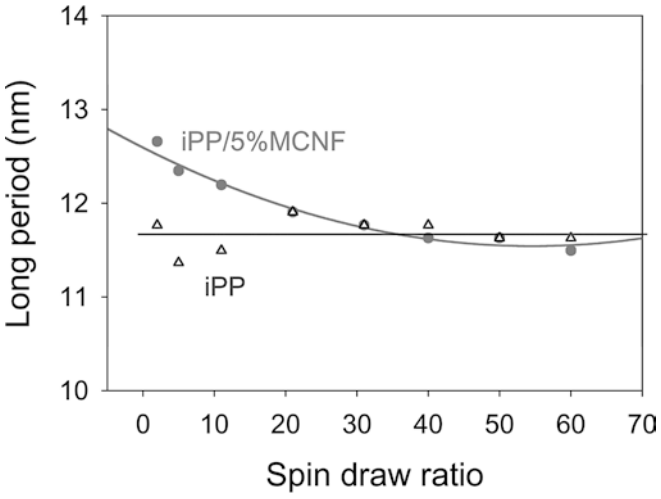

Fig. 7 Long periods of the nanocomposite and pure iPP fibers as a function of spin-draw ratio

spin-draw ratio. It was found that the nanocomposite fiber formed a larger long period at low spin-draw ratios. At high draw ratios, the long period of the composite fiber was similar to that of the pure iPP. We think that at low spin-draw ratios, relatively larger iPP lamellae are formed around the carbon nanofibers because short MCNFs are oriented first and act as nuclei. At high draw ratios, however, the nucleating effect of MCNFs is no longer dominant as the iPP chains can also be stretched and form even more effective nuclei.

On the equator, the pure iPP fiber showed a typical equatorial streak due to a fibrillar superstructure while the nanocomposite fiber showed a strong diamond shaped SAXS pattern.

The latter is most likely due to the oriented hollow cores of the CNFs, which provide the greater source of density contrast at the present length scales than the iPP superstructure.

A bundle of the spun fibers (pure and nanocomposite) with SDR of 50.0 was used to measure the tensile mechanical properties. Table 1 shows the tensile strength, Young's modulus and elongation-to-break of the nanocomposite and pure iPP fibers. It was found that the nanocomposite fiber with 5% MCNF had much higher tensile strength, modulus and elongation-to-break values. It was evident that the surface modification of carbon nanofibers successfully increased the interactions between carbon nanofiber and the iPP matrix, thereby enhancing the homogenous dispersion of the carbon nanofibers in the matrix and the mechanical performance. The morphological studies of the composite fiber confirmed this.

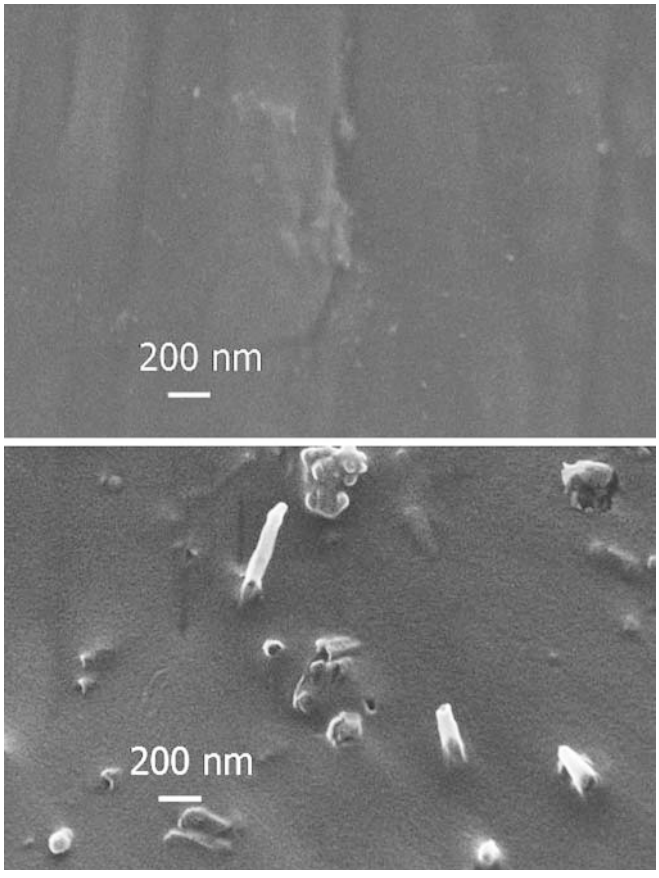

Fig. 8 SEM images of surface and cross-section of nanocomposite fibers

Figure 8 shows the SEM pictures of the surface and the cross-section of the nanocomposite fiber. It is found that the fiber surface is smooth. The cross-section clearly showed that the MCNFs were dispersed in the iPP matrix as separated fibers, not as bundled aggregates. This indicated that our surface modification was successful and the surface modified olefin layers might behave as "solvent" facilitating the dispersion of MCNF in the matrix during mixing.

Table 1 Mechanical properties of iPP and iPP/5% MCF nanocomposite fibers

	Pure iPP			iPP/5% MCF		
	Tensile strength (MPa)	Modulus (GPa)	Elongation (%)	Tensile strength (MPa)	Modulus (GPa)	Elongation (%)
Average	175 ± 20	2.87 ± 0.5	321 ± 40	319 ± 36	4.53 ± 0.7	533 ± 70

Conclusions

A nanocomposite system based on iPP and organic modified carbon nanofibers was prepared by blending 95 wt% iPP with 5 wt% MCNF. The modification of CNF consisted of a surface treatment by in-situ polymerization of olefin segments to make CNFs more compatible with the iPP matrix. The in-situ synchrotron SAXS and WAXD techniques were used to study the structural development of the nanocomposite fiber during melt-spinning. X-ray results showed that at low spin-draw ratios, the iPP/MCNF nanocomposite fiber exhibited much higher orientation of iPP crystals than the control iPP fiber. At higher spin-draw ratios, the orientation of the nanocomposite fiber and that of the pure iPP fiber were about the same. We think that the rigid carbon nanofibers behave as heterogeneous nucleating sites to induce the preferred packing of iPP crystalline chains along the drawing direction. However, this effect is less important at high spin-draw ratios, as the stretched oriented chains can form even more effective nuclei to induce crystallization of iPP. The crystallinity of the nanocomposite fiber was higher than that of the control fiber, which is a further consequence of the nucleation effect of MCNFs. The nanocomposite fiber also showed larger long periods at low spin-draw ratios.

Measurements of mechanical properties showed that the nanocomposite fiber with 5 wt% MCNF had much higher tensile strength, modulus and longer elongation-to-break values. It appeared that the surface modification of carbon nanofibers successfully increased the interactions between the carbon nanofibers and the iPP matrix, thereby enhancing the homogenous dispersion of the carbon nanofibers in the matrix (effective dispersion). The SEM images of the cross-section of the nanocomposite fiber clearly showed that the MCNFs were dispersed as isolated fibers, not a bundle, which confirmed our hypothesis. It appears that the primary reason for the changes in the mechanical properties of the iPP/MCNF nanocomposite fiber is due to the change of orientation and crystallinity properties of the polymer matrix, indicating a mostly indirect effect of the MCNF nanofiller rather than the more direct contributions of embedded fibers to the mechanical properties in classical fiber-reinforced polymer composites.

Acknowledgements The financial support of this work was provided by U.S. Army Research Office (DAAD190010419), the Department of Energy (DEFG0286ER45237.016 and DEFG0299ER45760), and the National Science Foundation (DMR9984102, DMR0098104) and ChemMat CARS by the National Science Foundation/DOE (CHE9522232, CHE0087817). The data analysis software (POLAR) was written by Dr. Dufei Fang at Stony Brook Technology and Applied Research Inc. (STAR).

References

1. Chen J, Rao AM, Lyuksyutov S, Itkis ME, Hamon MA, Hu H, Cohn RW, Eklund PC, Colbert DT, Smalley RE, Haddon RC (2001) J Phys Chem B 105:2525
2. Thostenson ET, Ren Z, Chou TW (2001) Compos Sci Technol 61:1899
3. Baker RTK, Harris PS (1978) In: Walker PL Jr, Thrower PA (eds) Chemistry and physics of carbon. Marcel Dekker, New York, vol 14, p 83
4. Oberlin A, Endo M, Koyama T (1976) J Cryst Growth 32:335
5. Dresselhaus MS, Dresselhaus G, Sugihara K, Spain IL, Goldberg HA (1988) Graphite fibers and filaments. Springer Series in Materials Science 5. Springer, Berlin Heidelberg New York
6. Rodriguez NM (1993) J Mater Res 8(12):3233
7. Kumar S, Doshi H, Srinivasarao M, Park JO, Schiraldi DA (2002) Polymer 43:1701
8. Lozano K, Barrera EV (2001) J Appl Polym Sci 79:125
9. Carneiro OS, Maia JM (2000) Polym Compos 21:961
10. Pogue RT, Ye J, Klosterman DA, Glass AS, Chartoff RP (1998) Composites Part A 29:1273
11. Hirsch A (2002) Angew Chem Int Ed 41(11):1853
12. Chen J, Rao AM, Lyuksyutov S, Itkis ME, Hamon MA, Hu H, Cohn RW, Eklund PC, Colbert DT, Smalley RE, Haddon RC (2001) J Phys Chem B 105:2525
13. Chen J, Hamon MA, Hu H, Chen Y, Rao AM, Eklund PC, Haddon RC (1998) Science 282:95
14. Hamon MA, Chen J, Hu H, Chen Y, Itkis ME, Rao AM, Eklund PC, Haddon RC (1999) Adv Mater 11:834
15. Holzinger M, Vostrowsky O, Hirsch A, Hennrich F, Kappes M, Weiss R, Jellen F (2001) Angew Chem 113:4132
16. Curran SA, Ajayan PM, Blau WJ, Carroll DL, Coleman JN, Dalton AB, Davey AP, Drury A, McCarthy B, Maier S, Strevens A (1998) Adv Mater 10:1091
17. Han W, Fan S, Li Q, Hu Y (1997) Science 277:1287
18. Ran S, Burger C, Fang D, Zong X, Cruz S, Hsiao BS, Chu B, Bubeck RA, Yabuki K, Teramoto Y, Martin DC, Johnson MA, Cunniff PM (2002) Macromolecules 35:433
19. Gravert DJ, Janda KD (1998) Tetrahedron Lett 39:1513
20. Friend SO, Barber JJ (1997) US Patent 5611964
21. Benoit D, Harth E, Fox P, Waymouth RM, Hawker CJ (2000) Macromolecules 33:363
22. Hahn SF (1992) J Polym Sci Part A Polym Chem 30:397
23. Alexander LE (1969) X-ray diffraction in polymer science. Wiley, New York, 582 pp